Synthesis and Preclinical Evaluation of ^{18}F-Labeled Ketoprofen Methyl Esters for Cyclooxygenase-1 Imaging in Neuroinflammation

Miho Shukuri*[1], Aya Mawatari*[2], Shuhei Takatani[2], Tsuyoshi Tahara[3,4], Michiko Inoue[3], Wakiko Arakaki[2], Masahiro Ohno[5], Hisashi Doi[2], and Hirotaka Onoe[6]

[1]*Laboratory of Physical Chemistry, Showa Pharmaceutical University, Tokyo, Japan;* [2]*Laboratory for Labeling Chemistry, RIKEN Center for Biosystems Dynamics Research, Hyogo, Japan;* [3]*Laboratory for Biofunction Dynamics Imaging, RIKEN Center for Biosystems Dynamics Research, Hyogo, Japan;* [4]*Department of in vivo Imaging, Advanced Research Promotion Center, Tokushima University, Tokushima, Japan;* [5]*Laboratory for Brain Connectomics Imaging, RIKEN Center for Biosystems Dynamics Research, Hyogo, Japan; and* [6]*Human Brain Research Center, Graduate School of Medicine, Kyoto University, Kyoto, Japan*

Cyclooxygenase (COX) is a rate-limiting enzyme in the synthesis of proinflammatory prostanoids from arachidonic acid. In vivo imaging of COX by PET is a potentially powerful tool for assessing the inflammatory response to injury, infection, and disease. We previously reported on a promising PET probe for COX imaging, ^{11}C-labeled ketoprofen methyl ester, which can detect COX-1 activation in models of neuroinflammation and neurodegenerative disorders. In the current study, we aimed to design a fluorine-substituted benzoyl group of ketoprofen (FKTP) and to evaluate its racemate and enantiomers (^{18}F-labeled ketoprofen methyl ester, [^{18}F]FKTP-Me) as PET proradiotracers, potential radiopharmaceuticals for in vivo PET study of COX-1. **Methods:** We performed nucleophilic aromatic ^{18}F-fluorination to obtain the desired racemic radiolabeled probe, (*RS*)-[^{18}F]FKTP-Me, at a radiochemical yield of 11%–13%. Subsequent high-performance liquid chromatography separation with a chiral column yielded the desired enantiomerically pure (*R*)- and (*S*)-[^{18}F]FKTP-Me. We examined the in vivo properties of (*RS*)-, (*R*)-, and (*S*)-[^{18}F]FKTP-Me in PET studies using rats in which hemispheric inflammation was induced by intrastriatally injecting a lipopolysaccharide. **Results:** Racemic (*RS*)-[^{18}F]FKTP-Me and enantiomeric (*R*)- or (*S*)-[^{18}F]FKTP-Me were synthesized with radiochemical and chemical purities of more than 99%. The metabolite analysis revealed that the racemic (*RS*)-[^{18}F]FKTP-Me crossed the blood–brain barrier and entered the brain, where it was subsequently hydrolyzed to its pharmacologically active acid form. PET images revealed a high accumulation of (*R*)-, (*S*)-, and (*RS*)-[^{18}F]FKTP in the inflamed regions in rat brain. Moreover, the accumulated radioactivity of (*S*)-[^{18}F]FKTP-Me was higher than that of (*RS*)-[^{18}F]FKTP-Me and (*R*)-[^{18}F]FKTP-Me, which was correlated with the stereospecific inhibitory activity of FKTP against COX-1. **Conclusion:** From the results of this study, we conclude that racemic (*RS*)-[^{18}F]FKTP-Me and its enantiomers could act as proradiotracers of neuroinflammation in rat brain by the association of their hydrolyzed acid forms with COX-1 in inflamed regions. In particular, (*S*)-[^{18}F]FKTP-Me demonstrated suitable properties as a COX-1–specific probe in PET imaging of neuroinflammation.

Key Words: COX-1; [^{18}F]FKTP-Me; neuroinflammation; PET

Received Dec. 22, 2021; revision accepted Mar. 2, 2022.

For correspondence or reprints, contact Hisashi Doi (hisashi.doi@riken.jp) or Hirotaka Onoe (h_onoe@kuhp.kyoto-u.ac.jp).

*Contributed equally to this work.

Published online Mar. 24, 2022.

COPYRIGHT © 2022 by the Society of Nuclear Medicine and Molecular Imaging.

J Nucl Med 2022; 63:1761–1767
DOI: 10.2967/jnumed.121.263713

Neuroinflammation is hypothesized to represent a pathologic cascade that leads to neurodegenerative diseases such as Alzheimer disease (AD) and Parkinson disease (*1*). The prostanoid-synthesizing enzymes cyclooxygenase (COX)-1 and -2 have been identified as principal targets for regulating neuroinflammation (*2,3*). Although COX-1 is constitutively expressed, COX-2 is induced in response to inflammatory stimuli in most tissues. The study findings to date indicate that the action of COXs in the brain is more complicated than expected. For example, clinical trials with COX-selective inhibitors such as nonsteroidal antiinflammatory drugs have yielded mixed results (*4–7*). Principally, COX-2–selective inhibitors have demonstrated null efficacy in the treatment of AD. Although COX-1–selective or –nonselective nonsteroidal antiinflammatory drugs (e.g., indomethacin and diclofenac) have shown beneficial trends in small clinical trials of AD treatment, they have produced mixed effects in larger, multicenter randomized controlled trials. Conversely, postmortem analyses have demonstrated upregulation of COX-1 within brain lesions in patients with AD or traumatic brain injury (*8,9*). There is some evidence that the inhibition or genetic ablation of COX-1 activity attenuates the inflammatory response and neurodegeneration (*3,10–12*). However, mechanisms underlying the role of COX-1 in regulating neuroinflammation in neurodegenerative conditions remain to be elucidated.

A noninvasive in vivo imaging method monitoring COX expression by PET could be a valuable tool for investigating the role of COX in neuroinflammation. ^{11}C-labeled methyl esters of 2-arylpropionic acids are useful as proradiotracers for neuroinflammation PET imaging, penetrating the blood–brain barrier and undergoing hydrolysis to their acidic form, which accumulates in inflamed brain regions in rat models (*13*). Moreover, ^{11}C-labeled ketoprofen methyl ester ([^{11}C]KTP-Me) could detect COX-1 expression in activated microglia (*14*).

Microglia are major regulators in neuroinflammation and have been implicated in the pathology of prevalent chronic and progressive neurodegenerative diseases (*15,16*). In studies on APP-Tg mice, the (*S*)-enantiomer of [^{11}C]KTP-Me, which had high specificity for

COX-1, effectively imaged increases in COX-1 in activated microglia, corresponding to amyloid plaque progression (*17*). Reports on [^{11}C]KTP-Me have raised the presumption that COX-1 plays a meaningful role in neuroinflammation and indicate its potency for imaging neuroinflammation targets.

We also focused on ^{18}F-labeled PET probes for COX-1, as these have highly specific radioactivity and a longer half-life than ^{11}C in clinical settings. Although there are reports of ^{18}F-labeled PET probes using several COX inhibitors, few probes have been found suitable for imaging neuroinflammation because of low penetration into the brain (*18,19*). [^{18}F]PS13 has been reported as a promising ^{18}F-labeled PET probe for COX-1 imaging in the brains of rhesus monkeys (*20*). However, studies on animal models of neuroinflammation or on human patients have not yet been reported. Hence, we aimed to synthesize and evaluate ^{18}F-incorporated ketoprofen methyl esters, its racemate (*RS*)-[^{18}F]FKTP-Me, and its enantiomers (*R*)-[^{18}F]FKTP-Me and (*S*)-[^{18}F]FKTP-Me in PET studies on a rat neuroinflammation model.

MATERIALS AND METHODS

Chemistry

In this study, 1-(3-bromophenyl)propan-1-one (**2**) was used as the starting material for preparing unradiolabeled fluorine–incorporated ketoprofen methyl esters ((*RS*)-FKTP-Me, (*R*)-FKTP-Me, and (*S*)-FKTP-Me) and 2-(4′-nitrobenzophenone-3-yl)propanoic acid methyl ester (**1**) for ^{18}F-labeling (Fig. 1). Initially, **2** underwent ketone rearrangement with hypervalent iodine (*21*) to generate 2-(3-bromophenyl)propanoic acid methyl ester (**3**). Palladium-catalyzed borylation of **3** resulted in pinacol borane-substituted substrate (**4**), which was hydrolyzed to produce boronic acid (**5**). Palladium-catalyzed cross-coupling (*22*) of **5** with 4-fluorobenzoic acid yielded the desired (*RS*)-FKTP-Me. A similar cross-coupling of **5** with 4-nitorobenzoic acid yielded **1**, a critical substrate for synthesizing ^{18}F-labeled FKTP-Me.

Enantiomerically pure unradiolabeled (*R*)- and (*S*)-FKTP-Me were obtained through the following procedure (Fig. 2). Initially, (*RS*)-FKTP-Me with a methyl ester structure was converted to carboxylic acid–structured (*RS*)-FKTP by hydrolysis. (*RS*)-FKTP was reacted with an optically resolving reagent, (*S*)- or (*R*)-3-methyl-2-phenylbutylamine (*23*), to produce diastereomeric ammonium salt; after 2 cycles of recrystallization, we obtained an enantiomerically pure acid form of (*R*)- or (*S*)-FKTP with 99% enantiomeric excess. Each absolute configuration of (*R*)- and (*S*)-FKTP was determined by circular dichroism spectroscopy, as compared with the spectra of reference compounds ((*R*)- and (*S*)-ketoprofen) with configurational correlations to (*R*)- and (*S*)-FKTP. (*R*)-FKTP showed a negative Cotton effect; (*S*)-FKTP showed a positive effect, in accordance with prior research (*24*). Methyl esterification of (*R*)- and (*S*)-FKTP under acidic conditions (avoiding racemization) produced the desired enantiomerically pure (*R*)- and (*S*)-FKTP-Me, respectively (99% enantiomeric excess). Procedural details are summarized in Supplemental Schemes 1–8 and Supplemental Figures 1–21 (supplemental materials are available at http://jnm.snmjournals.org).

Synthesis of (*RS*)-[^{18}F]FKTP-Me and Its Optical Resolution

Figure 3 depicts the process of (*RS*)-[^{18}F]FKTP-Me synthesis. Nucleophilic ^{18}F-fluorination of **1** was performed with [^{18}F]KF and Kryptofix 222 (Merck) in dimethyl sulfoxide at 120°C for 10 min, followed by semipreparative high-performance liquid chromatography (HPLC) purification (generating (*RS*)-[^{18}F]FKTP-Me). Synthesis was performed in 52–60 min. The radioactivity of (*RS*)-[^{18}F]FKTP-Me was 0.9–2.2 GBq, and its decay-corrected radiochemical yield was 11%–13% (based on [^{18}F]KF with a radioactivity of ~24 GBq). The molar activity was 63–246 GBq/μmol, and the radiochemical and chemical purities were each more than 99%.

We prepared single (*R*)-[^{18}F]FKTP-Me or (*S*)-[^{18}F]FKTP-Me enantiomers according to the optical resolution of (*RS*)-[^{18}F]FKTP-Me using HPLC with a chiral column (Fig. 3). (*RS*)-[^{18}F]FKTP-Me was isolated using HPLC, followed by optical resolution of (*RS*)-[^{18}F]FKTP-Me through a chiral HPLC method to produce ^{18}F-labeled (*R*)- and (*S*)-enantiomers (>99% enantiomeric excess). The total synthesis time, including ^{18}F-fluorination and optical resolution, was 70–92 min. The radioactivities of the (*R*)- and (*S*)-enantiomers were 400−528 MBq and 193–1,094 MBq, respectively. The respective molar activities were 63−91 GBq/μmol and 47–208 GBq/μmol. The respective [^{18}F]KF-based decay-corrected radiochemical yields for the (*R*)- and (*S*)-enantiomers were 1%–3% and 1%–6%. The radiochemical and chemical purities were more than 99%. Both probes met the criteria for in vivo animal experiments. Further details on the experimental conditions and procedures are described in Supplemental Schemes 9–10 and Supplemental Figures 22–25.

COX Inhibitory Activity

We measured the inhibitory activity of FKTP against recombinant COX-1 and -2 enzymes using a colorimetric COX (ovine) inhibitor screening assay kit (Cayman Chemical Co.) according to procedures described in the supplemental information.

Animals and Surgery

All experimental protocols were approved by the Animal Care and Use Committee of RIKEN Kobe Institute (approval MA2009-21-6) and were performed in accordance with the ARRIVE guidelines (Animal Research: Reporting of In Vivo Experiments). We used male Wistar rats (aged 10–13 wk) from CLEA Japan, Inc. for preparing the rat model of acute neuroinflammation; 3–4 rats were housed per cage under a 12-h light–dark cycle (lights off at 20:00) at 23°C ± 1°C and 60% ± 5% humidity. The rats were provided ad libitum access to food and water. We injected lipopolysaccharide (strain 026:B6; Sigma-Aldrich. Co. Ltd.) diluted in saline into the striatum (0.5 μg/μL, 0.2 μL/min for 5 min) using a 26-gauge needle controlled by an automated syringe pump (Muromachi Kikai Co., Ltd.) under sodium pentobarbital anesthesia (50 mg/kg). The stereotactic coordinates from the bregma were as follows: anteroposterior, +0.2 mm; lateral, +3.2 mm; and ventral, −5.5 mm (from the dura). After injection, the needle was left in place for 5 min before being slowly removed.

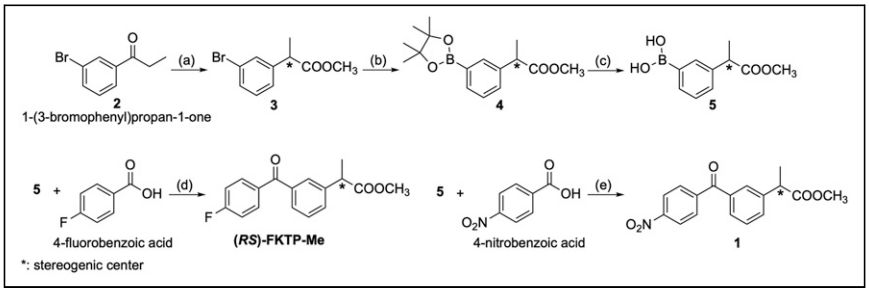

FIGURE 1. Preparation of (*RS*)-FKTP-Me and **1** for ^{18}F-labeling. (a) Hypervalent iodine-induced ketone rearrangement. (b) Palladium-catalyzed borylation. (c) Hydrolysis. (d and e) Palladium-catalyzed cross-coupling to build benzophenone structure.

PET Imaging

We performed PET studies on day 1 after lipopolysaccharide injection. The rats were anesthetized with a mixture of 1.5% isoflurane and nitrous oxide/oxygen (7:3) and placed on

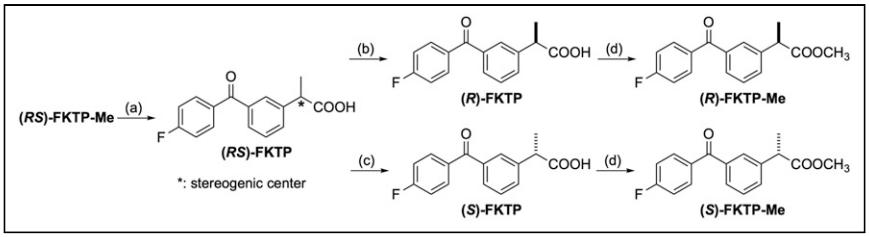

FIGURE 2. Synthesis of enantiomerically pure (*R*)-FKTP-Me and (*S*)-FKTP-Me. (a) Hydrolysis. (b and c) Optical resolution using (*S*)- and (*R*)-3-methyl-2-phenylbutylamine, respectively. (d) Esterification under acidic conditions.

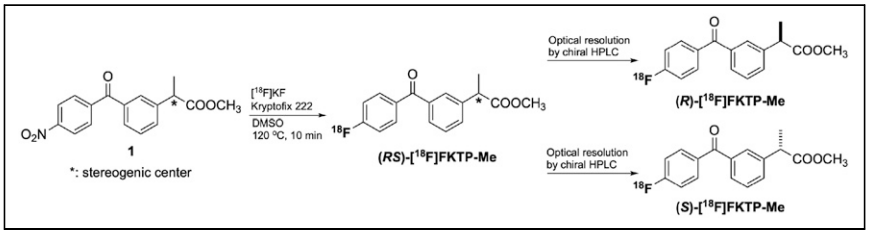

FIGURE 3. Synthesis of (*RS*)-[^{18}F]FKTP-Me, (*R*)-[^{18}F]FKTP-Me, and (*S*)-[^{18}F]FKTP-Me. DMSO = dimethylsulfoxide.

the bed of a small-animal PET scanner (microPET Focus-220; Siemens AG). (*RS*)-, (*R*)-, and (*S*)-[^{18}F]FKTP-Me (~50 MBq per animal) dissolved in 1 mL of saline were injected via the cannula inserted into the tail vein for 10 s, followed by the acquisition of emission data for 90 min using the 3-dimensional list-mode method. In the blocking studies, unlabeled (*RS*)-FKTP-Me (10 mg/kg) or (*S*)-FKTP-Me (10 mg/kg) was administered simultaneously with the PET probe. The molar activities and injected mass of (*RS*)-, (*R*)-, and (*S*)-[^{18}F]FKTP-Me at the time of administration were 94.2 ± 47.5 GBq/μmol (0.69 ± 0.32 nmol), 58.3 ± 24.9 GBq/μmol (0.85 ± 0.24 nmol), and 95.9 ± 44.8 GBq/μmol (0.49 ± 0.17 nmol), respectively. PET data were fused with T1-weighted MR images, and regions of interest were placed in the brain using image processing software (PMOD, version 3.4; PMOD Technologies Ltd.). Regional uptake was expressed as SUVs (tissue activity [MBq/g]/[injected dose (MBq)/body weight (g)]) (details are provided in the supplemental information).

Statistical Analyses

Statistical analyses were performed using the Student *t* test. *P* values of less than 0.05 were considered statistically significant.

RESULTS

Chemistry

We developed 6 unradiolabeled compounds of (*RS*)-, (*R*)-, and (*S*)-FKTP as acid forms, with (*RS*)-, (*R*)-, and (*S*)-FKTP-Me as methyl esters. The enantiomeric excess of 4 compounds ((*R*)-FKTP, (*S*)-FKTP, (*R*)-FKTP-Me, and (*S*)-FKTP-Me) was more than 99%.

Radiochemistry

We successfully synthesized the following radiolabeled probes: (*RS*)-[^{18}F]FKTP-Me, (*R*)-[^{18}F]FKTP-Me, and (*S*)-[^{18}F]FKTP-Me. These probes met the criteria for in vivo animal experiments (chemical purity, all >99%; radiochemical purity, all >99%; radioactivity, 0.19–2.2 GBq; molar activity, 47–246 GBq/μmol).

Inhibitory Activity of FKTP

The inhibitory activity of the (*S*)-enantiomer of FKTP was highly selective for COX-1 (COX-1/COX-2 ratio, 49.2). (*R*)-FKTP displayed less inhibitory activity against both COX-1 and COX-2 (COX-1/COX-2 ratio, 36.0) (Table 1). To examine the binding of FKTP toward COXs under in vivo conditions, we performed a blocking study using ex vivo autoradiography with (*S*)-[^{11}C]KTP-Me and (*RS*)-FKTP-Me. At 45 min after (*S*)-[^{11}C]KTP-Me injection, accumulated radioactivity in the rat brain on day 1 after lipopolysaccharide injection was decreased by the simultaneous administration of (*RS*)-FKTP-Me, indicating that (*RS*)-FKTP-Me entered the brain and displayed specificity for COX-1 under in vivo conditions (Supplemental Fig. 26).

PET Imaging of Neuroinflammation

PET images obtained by the summation of dynamic data for 5–45 min after (*RS*)-[^{18}F]FKTP-Me injection demonstrated high radioactivity accumulation in the ipsilateral cortex and striatum, compared with the contralateral side on day 1 after lipopolysaccharide injection (Fig. 4A). Immunohistochemical studies showed a statistically significant increase in COX-1–expressing activated microglia in the ipsilateral cortex and striatum (Supplemental Fig. 27). The distribution of high radioactivity in PET images with (*RS*)-[^{18}F]FKTP-Me was strongly correlated with increased accumulation of COX-1–expressing OX-42–positive activated microglia in inflamed regions. The time–activity curves of (*RS*)-[^{18}F]FKTP-Me demonstrated peak radioactivity accumulation within 1 min after injection in all brain regions (Fig. 4B). Although the radioactivity in the contralateral striatum or cerebellum was rapidly washed out (within 15 min), the ipsilateral striatum revealed a delay in clearance resulting in high accumulation. Simultaneous administration of unlabeled (*RS*)-FKTP-Me and (*RS*)-[^{18}F]FKTP-Me statistically significantly reduced radioactivity accumulation in the ipsilateral striatum (Table 2). Administering (*S*)-FKTP-Me decreased radioactivity accumulation in the ipsilateral striatum, but the difference was not statistically significant ($P = 0.054$).

Metabolic Analysis of (*RS*)-[^{18}F]FKTP-Me in Rat Tissues

We performed HPLC analysis using plasma and brain extracts at different time points after injecting (*RS*)-[^{18}F]FKTP-Me. Two minutes after injection, 1 metabolite peak appeared in the plasma sample, identified as (*RS*)-[^{18}F]FKTP (a hydrolyzed metabolite of (*RS*)-[^{18}F]FKTP-Me; Supplemental Fig. 28). Brain samples at

TABLE 1
Inhibitory Effects of Ketoprofen Enantiomers on Ovine COX-1 and COX-2 Activities

	50% inhibitory concentration (μM)	
Parameter	(*R*)-FKTP	(*S*)-FKTP
COX-1	4.50	0.127
COX-2	162	6.25

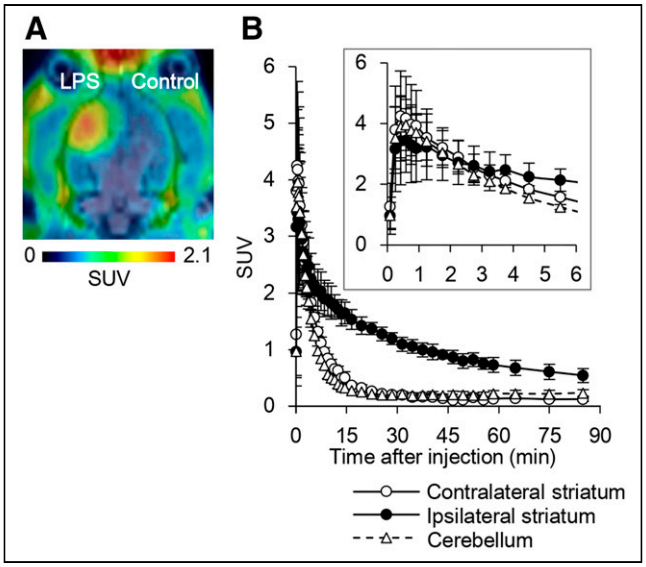

FIGURE 4. Representative PET images and time-radioactivity curves of (*RS*)-[^{18}F]FKTP-Me in rat brain after lipopolysaccharide (LPS) injection. (A) Transaxial rat brain views of SUV-summed PET image from 5 to 45 min after probe injection, coregistered with MR images. (B) Quantitative time-radioactivity curves of (*RS*)-[^{18}F]FKTP-Me in contralateral and ipsilateral (lipopolysaccharide-injected) striatum, and cerebellum. Truncated data of the first 6 min are shown in the inset. Data are expressed as SUVs and means ± SDs (n = 6).

2 min after injection revealed 2 peaks corresponding to (*RS*)-[^{18}F]FKTP-Me and (*RS*)-[^{18}F]FKTP. The metabolite component identified as (*RS*)-[^{18}F]FKTP-Me was lower in both the lipopolysaccharide-injected and the contralateral hemispheres at 5 min and was completely converted to (*RS*)-[^{18}F]FKTP until 10 min after injection (Fig. 5).

Stereospecificity of [^{18}F]FKTP-Me in PET Imaging

PET images on day 1 after lipopolysaccharide injection revealed that both (*R*)-[^{18}F]FKTP-Me and (*S*)-[^{18}F]FKTP-Me displayed high radioactivity accumulation in the inflamed regions, including ipsilateral cortex and striatum (Fig. 6A). The radioactivity uptake value after (*S*)-[^{18}F]FKTP-Me injection was higher than that of (*R*)-[^{18}F]FKTP-Me in all brain regions (Table 3). In the blocking study with (*S*)-KTP-Me, the blockade rate of (*S*)-[^{18}F]FKTP-Me in the ipsilateral striatum (30.1%) was higher than that of (*R*)-[^{18}F]FKTP-Me (21.3%). Time–activity curves of (*S*)-[^{18}F]FKTP-Me revealed that the peak was reached within 1 min of injection on the ipsilateral and contralateral sides, with comparable peak radioactivity in (*R*)-[^{18}F]FKTP-Me (Fig. 6B). The time to halve the radioactivity of (*S*)-[^{18}F]FKTP-Me in the ipsilateral striatum (∼20 min) was longer than that of (*R*)-[^{18}F]FKTP-Me (∼5 min), suggesting that (*S*)-[^{18}F]FKTP-Me displayed higher binding.

DISCUSSION

Previously, we reported that (*RS*)- and (*S*)-[^{11}C]KTP-Me specific to COX-1 are valuable PET probes for neuroinflammation, and we provided evidence for COX-1 as a surrogate marker for microglial activation (*14,17*). In the present study, we designed and evaluated [^{18}F]FKTP-Me as PET probes for clinical application. Our PET studies using rats with lipopolysaccharide-induced hemispheric neuroinflammation demonstrated specific accumulation of (*RS*)-[^{18}F]FKTP-Me, which was blocked by unlabeled (*RS*)-FKTP-Me or (*S*)-KTP-Me. Metabolic analysis revealed that (*RS*)-[^{18}F]FKTP-Me in the plasma was immediately converted to (*RS*)-[^{18}F]FKTP, an active form specifically accumulated in neuroinflammation. The hydrolysis rate in the brain was relatively slower than that in the plasma. At 2 min after (*RS*)-[^{18}F]FKTP-Me administration, (*RS*)-[^{18}F]FKTP-Me persisted in the ipsilateral and contralateral brain (22.7% and 31.2%, respectively); it was completely hydrolyzed to (*RS*)-[^{18}F]FKTP within 10 min of administration. Despite the hydrolysis rate of (*RS*)-[^{18}F]FKTP-Me possibly influencing accumulation, (*RS*)-[^{18}F]FKTP levels in the contralateral and ipsilateral brain did not display a statistically significant difference 2 min after administration ($P > 0.05$). Moreover, there were no differences in the initial uptake value between the ipsilateral and contralateral brain according to time–activity curves. In other words, the high accumulated radioactivity of (*RS*)-[^{18}F]FKTP-Me in neuroinflammatory regions should be related to an increase in binding to COX-1.

When the stereospecificity of [^{18}F]FKTP-Me was evaluated, (*S*)-[^{18}F]FKTP-Me displayed an increased radioactivity accumulation in all brain regions as compared with (*RS*)- and (*R*)-[^{18}F]FKTP-Me. Blocking studies with (*S*)-KTP-Me revealed specific radioactivity accumulation of both (*R*)-[^{18}F]FKTP-Me and (*S*)-[^{18}F]FKTP-Me. The highest blockade rate in the ipsilateral striatum was observed in

TABLE 2
Regional Brain Accumulation of (*RS*)-[^{18}F]FKTP-Me and Blockade by Simultaneous Administration of Unlabeled COX-1 Inhibitors

Site	Vehicle (n = 6)	(*RS*)-FKTP-Me (n = 4)	(*S*)-KTP-Me (n = 3)
Ipsilateral cortex	1.24 ± 0.29	1.12 ± 0.075	0.97 ± 0.22
Contralateral cortex	0.55 ± 0.032	0.67 ± 0.032*	0.60 ± 0.070
Ipsilateral striatum	1.35 ± 0.12	1.14 ± 0.066†	1.05 ± 0.29
Contralateral striatum	0.39 ± 0.027	0.50 ± 0.037*	0.45 ± 0.071
Cerebellum	0.32 ± 0.039	0.51 ± 0.062*	0.49 ± 0.030*

*$P < 0.001$ for vehicle vs. (*RS*)-FKTP-Me or (*S*)-KTP-Me.
†$P < 0.05$ for vehicle vs. (*RS*)-FKTP-Me or (*S*)-KTP-Me.
Absorbed doses of (*RS*)-[^{18}F]FKTP-Me were calculated using summed PET images from 5 to 45 min after probe injection and are expressed as SUV. Unlabeled (*RS*)-FKTP-Me (10 mg/kg) and (*S*)-KTP-Me (10 mg/kg) were administered simultaneously with (*RS*)-[^{18}F]FKTP-Me.

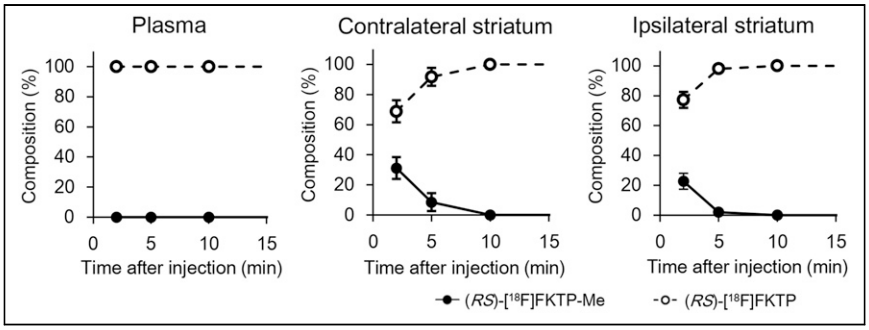

FIGURE 5. Plasma and brain compositions of (*RS*)-[^{18}F]FKTP-Me and its metabolite, (*RS*)-[^{18}F]FKTP. Data are expressed as means ± SDs (10 min, $n = 3$; others, $n = 4$).

(*S*)-[^{18}F]FKTP-Me (30.1%), as compared with (*R*)-[^{18}F]FKTP-Me (21.3%) and (*RS*)-[^{18}F]FKTP-Me (22.1%), suggesting the greater specificity of (*S*)-[^{18}F]FKTP-Me, corresponding to stereospecific inhibitory activities of FKTP against COX-1. A meaningful reduction caused by blocking in the ipsilateral cortex was observed for only (*S*)-[^{18}F]FKTP-Me. Neither (*R*)-[^{18}F]FKTP-Me nor (*RS*)-[^{18}F]FKTP-Me showed evidence of (*S*)-[^{18}F]FKTP-Me specificity.

A higher radioactivity accumulation of (*S*)-[^{18}F]FKTP-Me in the ipsilateral and contralateral hemispheres may suggest that (*S*)-[^{18}F]FKTP-Me shows high nonspecific accumulation. The (*S*)-[^{18}F]FKTP-Me/(*R*)-[^{18}F]FKTP-Me ratios were 1.63 and 1.69 in the ipsilateral and contralateral striata, respectively. Since COX-1 is known to be distributed throughout the brain even under normal conditions, a higher accumulation of (*S*)-[^{18}F]FKTP-Me in the contralateral hemisphere may include specific binding to COX-1. However, our blocking experiments showed no difference in the contralateral hemisphere. An incomplete blocking effect was also shown in the ipsilateral hemisphere with respect to (*RS*)-, (*R*)-, and (*S*)-[^{18}F]FKTP-Me, which corroborates our previous study findings for (*RS*)-[^{11}C]KTP-Me (*14*). A possible reason is that the dose of (*S*)-KTP-Me (10 mg/kg) used in blocking studies may not be sufficient to inhibit specific binding completely. Alternatively, disruption to brain structure may be caused by multiple inflammatory factors, including dysfunction of the blood–brain barrier produced by direct intrastriatal lipopolysaccharide injection.

An unexpected result was observed in comparing ipsilateral-to-contralateral radioactivity ratios. Specifically, the ratio of (*S*)-[^{18}F]FKTP-Me in the striatum (3.85 ± 0.35) was equivalent to that of (*R*)-[^{18}F]FKTP-Me (3.99 ± 0.48), which seemingly does not match the inhibitory activities of FKTP against COX-1. In our previous experiments, [^{11}C]KTP-Me showed similar ipsilateral-to-contralateral ratios in the striatum for (*R*)-[^{11}C]KTP-Me and was 1.3 times higher for (*S*)-[^{11}C]KTP-Me than for [^{18}F]FKTP-Me. The accumulation of (*R*)-[^{18}F]FKTP-Me in the contralateral striatum and cortex was lower than that of (*S*)-[^{18}F]FKTP-Me, despite being the same in the cerebellum, where COX-1 expression is low. The reason for this finding is unclear. However, because of some combination of factors, the ipsilateral-to-contralateral ratio of (*S*)-[^{18}F]FKTP-Me reached the same level as that of (*R*)-[^{18}F]FKTP-Me.

Slight but statistically significant increases in radioactivity accumulation in noninflamed regions (the contralateral cortex, striatum, and cerebellum) were observed in our blocking studies of (*R*)-[^{18}F]FKTP-Me and (*RS*)-[^{18}F]FKTP-Me with administration of (*S*)-KTP-Me or (*RS*)-KTP-Me. The phenomenon was seen only for (*R*)-[^{18}F]FKTP-Me and (*RS*)-[^{18}F]FKTP-Me, not for (*S*)-[^{18}F]FKTP-Me, and did not occur in the ipsilateral hemisphere. Since there was no difference in the initial uptake, it is unlikely that this effect was due to pharmacokinetic changes caused by the administration of the COX-1 inhibitor, such as increased cerebral blood flow. Although it is difficult to identify, the presence of unknown specific binding to (*R*)-[^{18}F]FKTP-Me may be involved in

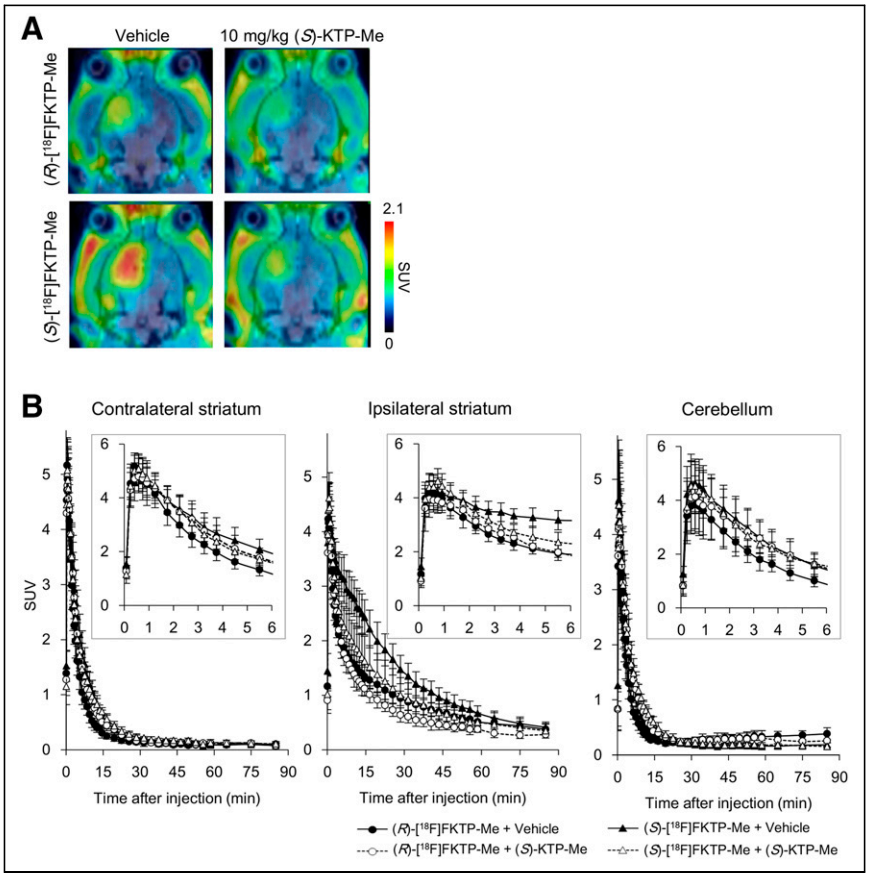

FIGURE 6. Representative PET images and time–radioactivity curves of (*R*)- and (*S*)-[^{18}F]FKTP-Me in rat brain after lipopolysaccharide injection with or without simultaneous (*S*)-KTP-Me administration. (A) Transaxial rat brain views of SUV-summed PET images from 5 to 45 min after probe injection, with or without administration of (*S*)-KTP-Me. (B) Quantitative time–radioactivity curves in evaluated brain regions. Data are expressed as SUVs and means ± SDs ((*R*)-[^{18}F]FKTP-Me + (*S*)-KTP-Me, $n = 3$; (*S*)-[^{18}F]FKTP-Me + (*S*)-KTP-Me, $n = 5$; others, $n = 6$).

TABLE 3
Regional Brain Accumulation of (*R*)- and (*S*)-[^{18}F]FKTP-Me and Blockade by Simultaneous Administration of (*S*)-KTP-Me

Site	(*R*)-[^{18}F]FKTP-Me		(*S*)-[^{18}F]FKTP-Me	
	Vehicle (n = 6)	(*S*)-KTP-Me (n = 3)	Vehicle (n = 6)	(*S*)-KTP-Me (n = 5)
Ipsilateral cortex	0.95 ± 0.18	0.81 ± 0.058	1.43 ± 0.26	1.00 ± 0.12*
Contralateral cortex	0.41 ± 0.062	0.51 ± 0.071	0.58 ± 0.10	0.61 ± 0.071
Ipsilateral striatum	1.11 ± 0.14	0.87 ± 0.14†	1.81 ± 0.28	1.27 ± 0.34†
Contralateral striatum	0.28 ± 0.051	0.41 ± 0.083†	0.48 ± 0.095	0.48 ± 0.056
Cerebellum	0.32 ± 0.037	0.44 ± 0.070†	0.35 ± 0.078	0.45 ± 0.069

*$P < 0.01$ vs. vehicle.
†$P < 0.05$ vs. vehicle.
Absorbed doses of (*R*)- and (*S*)-[^{18}F]FKTP-Me were calculated using summed PET images from 5 to 45 min after probe injection and are expressed as SUVs. Data are expressed as means ± SDs. Unlabeled (*S*)-KTP-Me (10 mg/kg) was simultaneously administered with (*R*)- or (*S*)-[^{18}F]FKTP-Me.

this phenomenon. In other words, it is assumed that (*R*)-[^{18}F]FKTP-Me–specific binding other than COX-1 was enhanced in an environment where binding to COX-1 was blocked by administering (*RS*)-FKTP-Me or (*S*)-KTP-Me. Also, the kinetics of (*R*)-[^{18}F]KTP-Me in the contralateral cortex and cerebellum showed increased radioactivity at a later phase (~30 min after injection) (Supplemental Fig. 29). This finding suggests the presence of different unknown metabolites in (*R*)-enantiomers, which could be evidence that (*R*)-[^{18}F]KTP-Me has a certain amount of nonspecific accumulation.

The present study demonstrated good properties of (*S*)-[^{18}F]FKTP-Me as a proradiotracer for imaging neuroinflammation, despite the lower inhibitory activity of (*S*)-FKTP against both COX-1 and COX-2 (vs. (*S*)-KTP; 50% inhibitory concentration for COX-1 and COX-2, 0.011 and 0.195 μM, respectively). Previously, we reported that [^{11}C]KTP-Me demonstrated a favorable dosimetry, biodistribution, and safety profile (*25*). However, the radioactivity of [^{11}C]KTP-Me was rapidly washed out from the cerebral tissue, and there was no obvious difference between healthy subjects and patients with mild cognitive impairment or AD (*26*). The characteristics of (*S*)-[^{18}F]FKTP-Me as a proradiotracer were consistent with those of (*S*)-[^{11}C]KTP-Me, but the initial uptake of (*S*)-[^{18}F]FKTP-Me shown in time–activity curves appeared to be higher than that of (*S*)-[^{11}C]FKTP-Me in our previous report. This difference may have contributed to the fact that PET images showed neuroinflammation with high sensitivity in the present study. Additional exploratory studies are expected to clarify the kinetics of (*S*)-[^{18}F]FKTP-Me in humans and demonstrate whether (*S*)-[^{18}F]FKTP-Me could be valuable for clinical applications in neurodegenerative disease.

CONCLUSION

The aim of the present study was to develop an ^{18}F-labeled PET imaging probe against COX-1 that can detect neuroinflammation, with clinical applications to diagnosing neurodegenerative disease. We established synthesis methods for (*RS*)-[^{18}F]FKTP-Me and its enantiomers, which demonstrated good brain penetration and accurate detection of neuroinflammation. (*S*)-[^{18}F]FKTP-Me was identified as a promising PET probe specific to COX-1 with respect to the imaging of neuroinflammation. Additional exploratory studies are necessary to confirm these findings more rigorously in both animal models and human subjects. However, we tentatively conclude that (*S*)-[^{18}F]FKTP-Me could be a candidate for future clinical applications in neurodegenerative diseases presenting with neuroinflammation. Our preliminary findings guide future research directions and may ultimately inform medical guidelines.

DISCLOSURE

This study was supported by the Molecular Imaging Research Program of Japan's Ministry of Education, Culture, Sports, Science, and Technology; the Research Center Network for Realization of Regenerative Medicine; the Agency for Medical Research and Development; and JSPS KAKENHI grant 15K09904. No other potential conflict of interest relevant to this article was reported.

ACKNOWLEDGMENTS

The experiments were performed at the RIKEN Center for Life Science Technologies. We thank Drs. Shunya Takahashi, Takemichi Nakamura, and Eiyu Imai (RIKEN CSRS) for providing compound characterization via circular dichroism spectral analysis and high-resolution mass spectrometry; Masahiro Kurahashi (Sumitomo Heavy Industry Accelerator Service Ltd.), Yasuhiro Wada, and Emi Hayashinaka (RIKEN BDR) for assisting with the PET studies; and Dr. Tadayuki Takashima (Pharmaceuticals Research Center, Asahi Kasei Pharma Corp.) for providing essential advice and technical information on metabolic analysis.

KEY POINTS

QUESTION: What is the potential for ^{18}F-labeled ketoprofen methyl esters ([^{18}F]FKTP-Me) to be applied as PET probes for COX-1 imaging in the brain?

PERTINENT FINDINGS: Racemic (*RS*)-[^{18}F]FKTP-Me and its enantiomers were successfully synthesized and demonstrated good brain penetration and COX-1–specific accumulation according to their hydrolyzed acidic form in rat brains. (*S*)-[^{18}F]FKTP-Me was identified as a PET probe with high specificity for COX-1 in the imaging of neuroinflammation.

IMPLICATIONS FOR PATIENT CARE: (*S*)-[^{18}F]FKTP-Me could be a promising candidate for diagnosis and basic research with regard to the role of COX-1 in neurodegenerative diseases.

REFERENCES

1. Wendeln A-C, Degenhardt K, Kaurani L, et al. Innate immune memory in the brain shapes neurological disease hallmarks. *Nature.* 2018;556:332–338.
2. Phillis JW, Horrocks LA, Farooqui AA. Cyclooxygenases, lipoxygenases, and epoxygenases in CNS: their role and involvement in neurological disorders. *Brain Res Brain Res Rev.* 2006;52:201–243.
3. Choi S-H, Aid S, Bosetti F. The distinct roles of cyclooxygenase-1 and -2 in neuroinflammation: implications for translational research. *Trends Pharmacol Sci.* 2009; 30:174–181.
4. McGeer PL, McGeer EG. NSAIDs and Alzheimer disease: epidemiological, animal model and clinical studies. *Neurobiol Aging.* 2007;28:639–647.
5. Vlad SC, Miller DR, Kowall NW, Felson DT. Protective effects of NSAIDs on the development of Alzheimer disease. *Neurology.* 2008;70:1672–1677.
6. Martin BK, Szekely C, Brandt J, et al.; ADAPT Research Group. Cognitive function over time in the Alzheimer's Disease Anti-inflammatory Prevention Trial (ADAPT): results of a randomized, controlled trial of naproxen and celecoxib. *Arch Neurol.* 2008;65:896–905.
7. de Jong D, Jansen R, Hoefnagels W, et al. No effect of one-year treatment with indomethacin on Alzheimer's disease progression: a randomized controlled trial. *PLoS One.* 2008;3:e1475.
8. Hoozemans JJ, Rozemuller AJ, Janssen I, De Groot CJ, Veerhuis R, Eikelenboom P. Cyclooxygenase expression in microglia and neurons in Alzheimer's disease and control brain. *Acta Neuropathol (Berl).* 2001;101:2–8.
9. Schwab JM, Seid K, Schluesener HJ. Traumatic brain injury induces prolonged accumulation of cyclooxygenase-1 expressing microglia/brain macrophages in rats. *J Neurotrauma.* 2001;18:881–890.
10. Gu X-L, Long C-X, Sun L, Xie C, Lin X, Cai H. Astrocytic expression of Parkinson's disease-related A53T alpha-synuclein causes neurodegeneration in mice. *Mol Brain.* 2010;3:12.
11. Choi S-H, Aid S, Caracciolo L, et al. Cyclooxygenase-1 inhibition reduces amyloid pathology and improves memory deficits in a mouse model of Alzheimer's disease. *J Neurochem.* 2013;124:59–68.
12. Griffin ÉW, Skelly DT, Murray CL, Cunningham C. Cyclooxygenase-1-dependent prostaglandins mediate susceptibility to systemic inflammation-induced acute cognitive dysfunction. *J Neurosci.* 2013;33:15248–15258.
13. Takashima-Hirano M, Shukuri M, Takashima T, et al. General method for the ^{11}C-labeling of 2-arylpropionic acids and their esters: construction of a PET tracer library for a study of biological events involved in COXs expression. *Chem.* 2010; 16:4250–4258.
14. Shukuri M, Takashima-Hirano M, Tokuda K, et al. In vivo expression of cyclooxygenase-1 in activated microglia and macrophages during neuroinflammation visualized by PET with ^{11}C-ketoprofen methyl ester. *J Nucl Med.* 2011;52:1094–1101.
15. Jin X, Yamashita T. Microglia in central nervous system repair after injury. *J Biochem (Tokyo).* 2016;159:491–496.
16. Saitgareeva AR, Bulygin KV, Gareev IF, Beylerli OA, Akhmadeeva LR. The role of microglia in the development of neurodegeneration. *Neurol Sci.* 2020;41: 3609–3615.
17. Shukuri M, Mawatari A, Ohno M, et al. Detection of cyclooxygenase-1 in activated microglia during amyloid plaque progression: PET studies in Alzheimer's disease model mice. *J Nucl Med.* 2016;57:291–296.
18. McCarthy TJ, Sheriff AU, Graneto MJ, Talley JJ, Welch MJ. Radiosynthesis, in vitro validation, and in vivo evaluation of ^{18}F-labeled COX-1 and COX-2 inhibitors. *J Nucl Med.* 2002;43:117–124.
19. Prabhakaran J, Molotkov A, Mintz A, Mann JJ. Progress in PET imaging of neuroinflammation targeting COX-2 enzyme. *Molecules.* 2021;26:3208.
20. Taddei C, Morse CL, Kim M-J, et al. Synthesis of [^{18}F]PS13 and evaluation as a PET radioligand for cyclooxygenase-1 in monkey. *ACS Chem Neurosci.* 2021;12: 517–530.
21. Malmedy F, Wirth T. Stereoselective ketone rearrangements with hypervalent iodine reagents. *Chem.* 2016;22:16072–16077.
22. Kakino R, Narahashi H, Shimizu I, Yamamoto A. Palladium-catalyzed direct conversion of carboxylic acids into ketones with organoboronic acids promoted by anhydride activators. *Bull Chem Soc Jpn.* 2002;75:1333–1345.
23. Chikusa Y, Fujimoto T, Ikunaka M, et al. (*S*)-3-methyl-2-phenylbutylamine, a versatile agent to resolve chiral, racemic carboxylic acids. *Org Process Res Dev.* 2002;6:291–296.
24. Blanco M, Coello J, Iturriaga H, Maspoch S, Pérez-Maseda C. Circular dichroism spectra of cyclodextrins–ketoprofen inclusion complexes: determination of enantiomeric purity. *Anal Chim Acta.* 2000;407:233–245.
25. Ohnishi A, Senda M, Yamane T, et al. Human whole-body biodistribution and dosimetry of a new PET tracer, [^{11}C]ketoprofen methyl ester, for imagings of neuroinflammation. *Nucl Med Biol.* 2014;41:594–599.
26. Ohnishi A, Senda M, Yamane T, et al. Exploratory human PET study of the effectiveness of ^{11}C-ketoprofen methyl ester, a potential biomarker of neuroinflammatory processes in Alzheimer's disease. *Nucl Med Biol.* 2016;43:438–444.